Catena 264 (2026) 109821

Contents lists available at ScienceDirect

Catena

journal homepage: www.elsevier.com/locate/catena

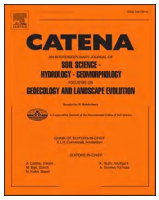

Hydrological alterations induced lakeward expansion of wetland vegetation in Dongting Lake, China's second-largest lake☆

Jiangjie Yang [a], Zhijun Dai [a,b,*], Xuefei Mei [a], Fangyuan Bu [a], Yizhuang Liu [c]

[a] State Key Laboratory of Estuarine and Coastal Research, East China Normal University, Shanghai 200062, China
[b] Laboratory for Marine Geology, Qingdao Marine Science and Technology Center, Qingdao 266061, China
[c] School of Hydraulic and Environmental Engineering, Changsha University of Science & Technology, Changsha 410114, China

ARTICLE INFO

Dataset link: Landsat5/7/8/9 and Sentinel-2 (Original data)

Keywords:
Vegetation expansion
Hydrological alteration
Lake wetlands
Dongting Lake

ABSTRACT

Dongting Lake (DTL), one of China's largest freshwater lakes and a critical wetland ecosystem, has shrunk rapidly due to both natural and human factors. This study presents one of the longest continuous analyses of wetland vegetation dynamics from 1989 to 2023 by combining long-term hydrological data with high-resolution remote sensing imagery, explicitly examining the impacts of hydrological alterations before and after the construction of the Three Gorges Dam (TGD). Results revealed that the vegetation area of DTL increased at a rate of 5.08 km^2/yr, with regional rates of 1.88 km^2/yr (East), 2.54 km^2/yr (South), and 1.46 km^2/yr (West), advancing lakeward at average rates of 27.56 ± 27.03 m/yr (East), 13.74 ± 14.45 m/yr (South), and 22.45 ± 20.67 m/yr (West), corresponding with water retreat and a downward shift of vegetation zones. Hydrological alterations caused by the TGD, including lower water levels (~0.6 m) and longer dry seasons (35 days), strongly shaped wetland vegetation dynamics, with East DTL mainly responding to water level decline and South and West DTL being more sensitive to dry season duration. Sediment input supported vegetation expansion, and vegetation-sediment feedback accelerated wetland evolution by trapping sediments and raising floodplain elevation. Local reclamation and sand mining resulted in a substantial wetland loss of 117.7 km^2. This study provides a comprehensive understanding of the coupled effects of hydrological drivers and ecological feedback on wetland evolution, offering critical insights for the sustainable management and restoration of lake ecosystems.

1. Introduction

As vital components of global inland ecosystems, lake wetlands provide essential services, such as flood regulation, water purification, biodiversity preservation, carbon sequestration, and freshwater retention (Ramsar Convention on Wetlands, 2018; Reynaud and Lanzanova, 2017; Sterner et al., 2020). Within these ecosystems, wetland vegetation, including emergent vegetation and trees, plays a crucial role in maintaining ecological integrity by supporting diverse wildlife and acting as a natural buffer against flooding and erosion, thereby enhancing ecosystem resilience to extreme weather events (Deng et al., 2014). Given their critical role, changes in wetland vegetation are widely recognized as key indicators of aquatic environmental security and wetland sustainability, while also among the most immediate signs of wetland degradation and succession (Tan et al., 2022; Liu et al., 2024).

In terms of global trends, lake wetlands have become some of the most endangered ecosystems, facing significant shrinkage and degradation in the context of intensified climate change and human activities (Asselen et al., 2013; Mei et al., 2016; Bu et al., 2025). It is estimated that more than half of the world's large lakes have experienced significant deterioration (Yao et al., 2023), as seen in the Great Lakes region (USA) (Gehring et al., 2020), Lake Victoria (Africa) (Nyamweya et al., 2023), and Lake Chad (Africa) (Grove, 1996). Since 1900, substantial loss of lake wetlands and vegetation has been observed (Davidson, 2014; Xu et al., 2023). In the Great Lakes region, 60–80% of lake wetlands have been lost since the 1800s (Kim et al., 2021). Similar losses are evident in China, where lake wetlands in the Changjiang River Plain have declined by over 11,800 km^2 during the past century (Li et al., 2024).

While wetland loss is the dominant global trend, some river-connected lakes exhibit vegetation expansion. This counterintuitive pattern, particularly in degraded or hydrologically altered lakes, may reflect ecological stress rather than recovery, as the expansion of

☆ This article is part of a Special issue entitled: 'Sediments and ecology' published in Catena.
* Corresponding authors.

https://doi.org/10.1016/j.catena.2026.109821
Received 14 June 2025; Received in revised form 4 November 2025; Accepted 8 January 2026
Available online 14 January 2026

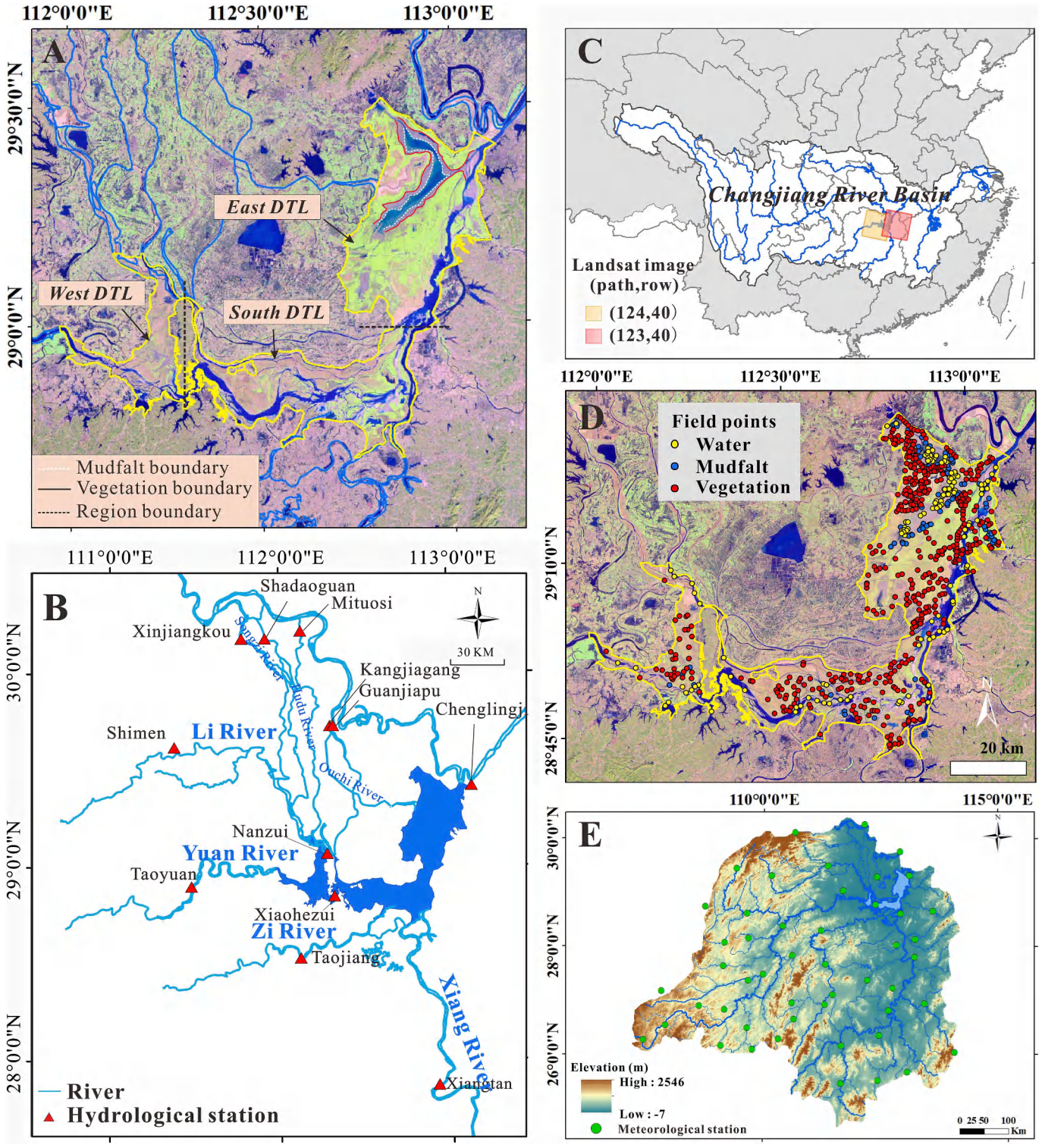

Fig. 1. Study map. A. Map of Dongting Lake (DTL); B. Tributaries and control hydrological stations of DTL; C. Location of DTL; D. Spatial distribution of field points for validation; E. Meteorological stations in DTL basin.

emergent vegetation can reduce open-water habitats, weaken hydrological connectivity, and accelerate succession-driven habitat loss (Mei et al., 2016). In China's large lakes, for instance, the vegetation area increased by 15.5% in Poyang Lake between 1989 and 2017 (Mu et al., 2020), and by about 80 km^2 in East Dongting Lake (DTL) from 1995 to 2015 (Hu et al., 2018). These vegetation expansions are frequently linked to altered hydro-sedimentary conditions, such as water-level fluctuations (Huang et al., 2024), sedimentation (Xie and Chen, 2008), and prolonged exposure periods (Mu et al., 2020; Yang et al., 2020), as well as climate drivers including precipitation, temperature, and solar radiation (Jiang et al., 2011; Zhang et al., 2021). Wang et al. (2024) emphasized that precipitation and temperature influence wetland vegetation by modifying hydrological conditions, while Liu et al. (2020) highlighted the coupling effect of climate and hydrological changes on wetland vegetation. Under escalating climate change and human pressures, such interactions increasingly drive rapid and complex

transformations in lake wetland vegetation dynamics.

As China's second-largest freshwater lake, DTL is designated as a Ramsar Wetland of International Importance and serves as a typical river-connected system that interacts closely with the Changjiang River, providing an ideal case study for investigating highly dynamic wetland vegetation (Xie et al., 2014; Liu et al., 2024; Guo et al., 2022). DTL is a throughflow-type lake, receiving inflow from the Changjiang River via the Three Inlets and from the Four Waters within its basin, before eventually discharging back into the Changjiang. This bidirectional river-lake exchange sustains extensive lacustrine floodplains and offers a unique opportunity to investigate the influence of declining water levels on wetland vegetation dynamics. Previous remote sensing studies on DTL have provided valuable insights into vegetation changes, particularly regarding general trends in wetland area (Yang et al., 2020; Peng et al., 2022; Liu et al., 2024). Meanwhile, extensive research has focused on variations in water surface and sediment deposition (Huang et al., 2012; Yu et al., 2018), as well as fluctuations in water level (Peng et al., 2005; Han et al., 2016; Yuan et al., 2015). However, the mechanisms through which hydrological alterations drive vegetation dynamics remain insufficiently understood.

This study therefore addresses these key knowledge gaps regarding the mechanisms of vegetation expansion in shrinking lake systems, with a particular focus on the role of hydrological alterations in DTL. We leverage a uniquely long time series from 1989 to 2023, combining Landsat TM/ETM+/OLI and Sentinel-2 imagery with daily hydrological and sediment data to document wetland vegetation dynamics in DTL. This dataset enables us to examine wetland vegetation responses to hydrological alterations, including comparisons between the pre- and post-Three Gorges Dam (TGD) periods. Thereafter, our study seeks to answer how hydrological alterations have influenced vegetation expansion in DTL. Our objectives are to: (1) monitor the hydro-sediment dynamic changes of DTL; (2) investigate the temporal and spatial change processes of wetland vegetation of DTL; and (3) diagnose the driving factors of wetland vegetation dynamics. Our findings contribute to a better understanding of wetland vegetation dynamics under altered hydrological regimes and offer guidance for the adaptive wetland management of large river-connected lakes.

2. Methods and materials

2.1. Study area

DTL (28°42′N-29°32′N, 111°52′E-113°08′E), China's second-largest freshwater lake, covers an area of approximately 2600 km^2. Located in a subtropical monsoon climate zone, it experiences notable seasonal rainfall variations, with the majority of precipitation occurring from April to June (Wang et al., 2011). The average annual air temperature ranges between 16.4–17.0 °C, and annual precipitation varies from 1100 to 1400 mm (Yin et al., 2022). Water level in DTL exhibits significant seasonal fluctuations, with intra-annual variations ranging from 6.6 to 15.4 m. Under the influence of seasonal water level fluctuations, DTL has developed a distinct wetland landscape characterized by a spatial zonation of open water, mudflats, and vegetation. This pattern exhibited an irregular strip or ring distribution along the elevation gradient (Jing et al., 2020). Herein, wetland vegetation (excluding aquatic vegetation.) is zonally distributed from the lake center toward the edge, consisting primarily of *Carex brevicuspis*, *P. australis*, *Populus nigra*, etc., with *P. australis* and *Carex brevicuspis* communities being dominant (Zhu et al., 2021; Peng et al., 2022). These vegetation types exhibit distinct a clear elevation-dependent distribution: *Carex brevicuspis* is primarily found in low-lying, seasonally inundated mudflats; *P. australis* is widely distributed in intermediate elevations, adapting to periodic water level fluctuations; while *P. nigra* typically grows at higher elevations, near the lake's edge or on alluvial plains. This elevation-based vegetation zonation reflects species-specific adaptations to hydrological conditions and the influence of seasonal water level variations.

According to the Ramsar convention classification, the DTL wetland is divided into three subregions, East, South, and West DTL (Fig. 1A). DTL wetland receives water and sediments from the Three Inlets (Songzi, Hudu, and Ouchi River) and the Four Waters (Xiang, Zi, Yuan, and Li Rivers), with its outflow eventually entering into the Changjiang River via Chenglingji station (Fig. 1B). These subbasins are nourished by different tributaries: East DTL is mainly influenced by the Ouchi River; South DTL is primarily nourished by the Xiang and Zi Rivers; and West DTL receives water and sediment from the Yuan, Li, Songzi, and Hudu Rivers.

2.2. Data sources

This study utilized four groups of data. The first group included remote sensing images, with one to two cloud-free images per year were acquired from the Google Earth Engine (GEE) platform, including Landsat imagery (TM, ETM+, and OLI sensors) from 1989 to 2015 and Sentinel-2 MSI imagery from 2016 to 2023. All datasets are Level-2 surface reflectance products (LANDSAT/LT05/C02/T1_L2, LANDSAT/LE07/C02/T1_L2, LANDSAT/LC08/C02/T1_L2, COPERNICUS/S2) with atmospheric and radiometric corrections applied, ensuring consistency and comparability across sensors and acquisition periods. To minimize seasonal and water-level influences on wetland classification, 1–2 scene images were selected per year during the dry season (October to February) at similar water levels (recorded at Chenglingji) to represent the annual wetland condition of DTL (Table S1). For Landsat images, the DTL requires two scenes for complete coverage (Fig. 1C). Specifically, East DTL and South DTL are mainly covered by the image path 123/row 40, with small portions falling within path 124/row 40, while West DTL is entirely covered by the image path 124/row 40 (Table S1). In contrast, a single Sentinel-2 scene per year provides full coverage of all three subregions (Table S1).

The second group is hydrological data, including water level, water discharge, suspended sediment discharge (SSD), and transect elevation, which were collected from the Changjiang Water Resources Commission (CWRC, http://www.cjw.gov.cn/). The daily water level at Chenglingji station served as the reference for the water levels of the entire lake. To account for spatial differences, we collected daily water levels from Xiaohezui and Chenglingji stations between October and February to assess their correlation across the eastern, southerb, and western subregions (Fig. S1). Daily water discharge and SSD from 1989 to 2022 were obtained from multiple hydrology stations: Chenglingji, Xiangtan, Taojiang, Taoyuan, Shimen, Xinjiangkou, Shadaoguan, Mituosi, Kangjiagang, and Guanjiapu. Annual water discharge and SSD were calculated by aggregating daily values (see detailed formulas in Supplementary Information). Values for the Three Inlets and Four Waters were calculated by summing the data from their respective controlling stations. Annual inflow of DTL was determined as the sum of the Four Waters and Three Inlets, while the outflow was based on data from Chenglingji station. Additionally, transect elevation data at Chenglingji and Nanzui in 2007, 2013, and 2020 were compiled to assess riverbed incision.

The third group comprises field validation data, categorized into three types: water, mudflat, and vegetation. These data were derived from historical imagery on Google Earth and published literature (Long et al., 2021; Peng et al., 2022). The spatial distribution of field validation data is shown in Fig. 1D.

The fourth group includes daily precipitation and temperature data of 35 stations over the DTL basin for the period 1989–2020, sourced from the China Meteorological Data Sharing Service System (https://data.cma.cn/). The spatial distribution of these stations is shown in Fig. 1E.

2.3. Methods

This study employed a cloud-based processing on GEE for scalable and reproducible classification, applied a Random Forest algorithm with

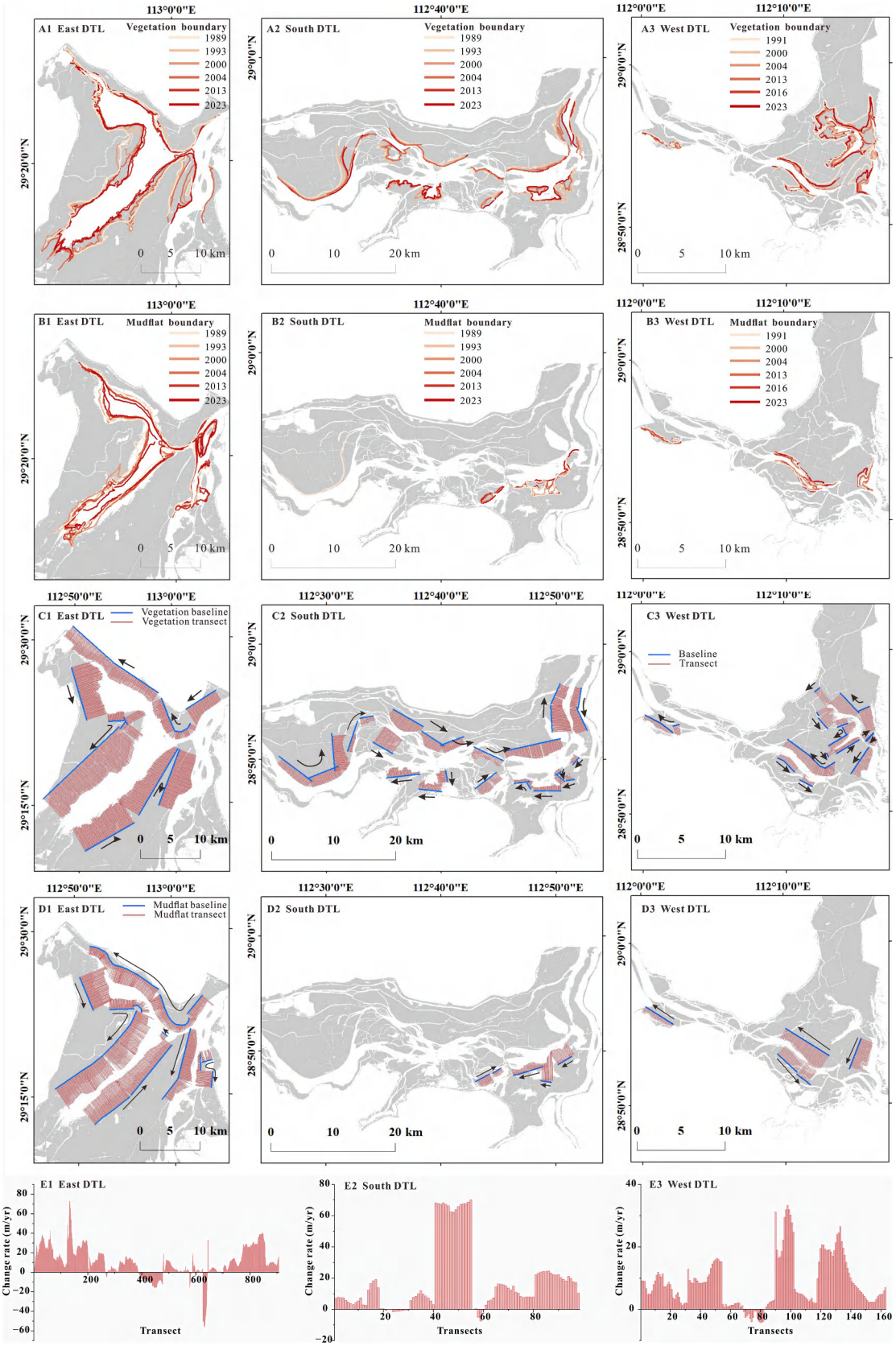

Fig. 2. Changes in boundary of vegetation (A) and mudflat (B) in three subregions. Transect settings of in vegetation (C) and mudflat (D) in three subregions. E. Change rate of mudflat boundary in three subregions. Panels 1–3 correspond to the East DTL, South DTL, and West DTL, respectively.

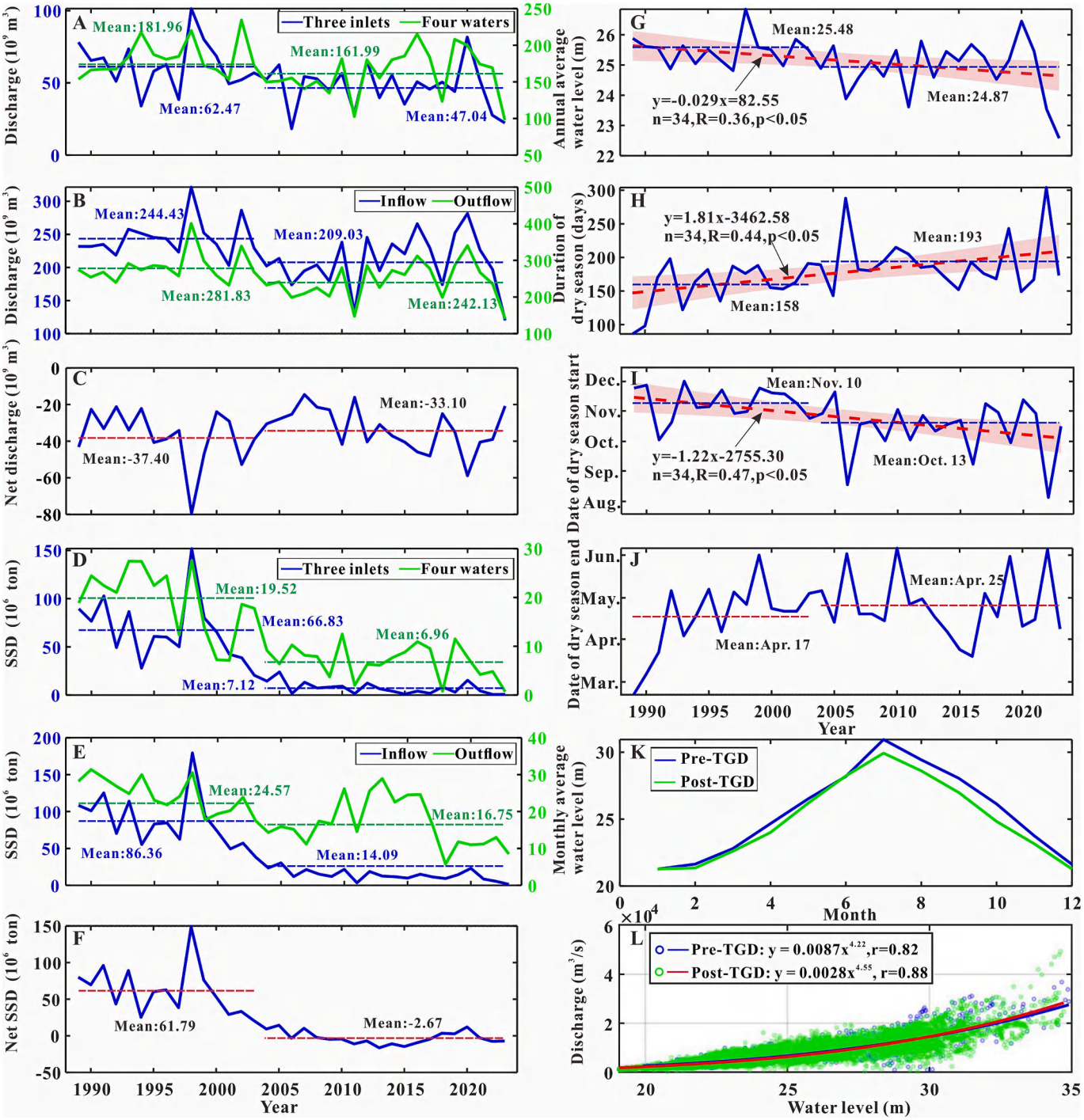

Fig. 3. Hydrological alteration. A. Annual water discharge at Three Inlets and Four Waters; B. Water inflow (sum of Three Inlets and Four Waters) and outflow (Chenglingji); C. Net water budget (the difference between inflow and outflow); D. SSD at Three Inlets and Four Waters; E.SSD input (sum of Three Inlets and Four Waters) and outflow (Chenglingji); F. Net sediment budget (the difference between inflow and outflow); G. Annual average water level; H. Duration of dry season; I. Date of dry season start; J. Date of dry season end; K. Monthly mean water level; L. Relationship of water level and discharge.

multi-spectral indices to distinguish water, mudflat, and vegetation, and used the Digital Shoreline Analysis System (DSAS) to quantify vegetation boundary changes over 35 years.

2.3.1. *Statistical analyses*

To evaluate temporal trends in vegetation area, both non-parametric and parametric statistical approaches were employed. First, the Mann–Kendall test was applied to detect monotonic trends in the time series, as it is widely used for hydrological and ecological data due to its robustness against non-normality and missing values (Mann, 1945; Kendall, 1970; Fig. S2). Second, linear regression analysis was performed to quantify the rate of vegetation area change. The regression slope and intercept were derived, and their statistical significance was assessed by *p*-values, while 95% confidence intervals were calculated to indicate the uncertainty of the estimated trends. Additionally, the relationships between climate/hydrological parameters (precipitation, water level, and duration of dry season) and vegetation metrics were quantified using Pearson correlation coefficients. These correlations

were visualized in a heatmap to facilitate the interpretation of the relative influence of hydrological factors on vegetation dynamics (Fig. S3). To compare the relative contributions of driven factors to vegetation area dynamics, standardized multiple linear regression model was also applied, with details provided in the Supplementary Materials (Table S8).

2.3.2. Hydrological definitions

According to the IPCC Fourth Assessment Report, an extreme hydrological event is defined as the occurrence of a value above the 75th (or below the 25th) percentile of a weather or climate variables (Intergovernmental Panel on Climate Change (IPCC), 2007). Specifically, a daily water level below the 25th percentile is considered as a low water level while a level above the 75th percentile is considered as a flood water level. In this study, the dry season of DTL is defined as the period when the daily water level at Chenglingji remains continuously below the 25th percentile threshold for a low water level (about 24.5 m), with percentiles calculated from the full study period. Furthermore, a significant shift in the hydrological regimes of the DTL was detected around 2003 based on the Mann-Kendall test, thus the study period was divided into two phases: pre-2003 and post-2003 (Fig. S2).

2.3.3. Image classification

The GEE cloud-based platform facilitates high-performance computing resources for large-scale geoscience analysis by invoking abundant databases and algorithms (Gorelick et al., 2017). All selected images listed in Table S1 were processed on the GEE platform (client library version 1.6.3). These Level-2 surface reflectance products had already undergone atmospheric and radiometric corrections. To minimize cloud contamination, clouds and cloud shadows were masked for all images. For Landsat images, the QA_PIXEL band was used following the official bitmask procedure, while for Sentinel-2 images, clouds and cloud shadows were masked using the QA60 band.

Following preprocessing, we applied the Random Forest algorithm implemented in GEE for wetland classification (Xing et al., 2022). For each annual image, hundreds of polygons representing water bodies, mudflats, and vegetation were delineated through visual interpretation. Within each polygon, 1000 random points per category were generated using the GEE command 'ee.FeatureCollection.randomPoints()'. This procedure constrained the sample points spatially within the delineated polygons, ensuring representative sampling across all wetland types. Random sampling of training points was performed and the coordinate reference system was set to EPSG:4326. Five spectral bands along with three spectral indices were used as input features for the Random Forest classifier (Table S2). Herein, the Random Forest classification in GEE was implemented using 100 trees, with default settings of equal class weighting and majority-vote strategy. Ultimately, a confusion matrix and evaluation metrics (overall accuracy and kappa coefficient) were used for validation. Class-specific accuracy, overall accuracy and kappa coefficient all exceeded 85% for each year during the classification process (Table S3–4), indicating the results are reliable (Arono, 1985; Congalton, 1991). Due to differences in satellite scene coverage, classification and accuracy assessment were conducted separately for each subregion. Consequently, overall accuracy and kappa values varied among subregions, even for images acquired on the same date.

Visual interpretation was employed to differentiate newly formed water bodies (ponds) resulting from sand mining or the 'return land to the lake' initiative, where land is abruptly transformed into ponds or open water. These emergent aquatic features were manually delineated, and their areas were computed using ArcGIS 10.7.

2.3.4. Boundary-change analysis

The evolution of wetland boundaries over the study period was quantified using the Digital Shoreline Analysis System (DSAS, version 5.1, https://code.usgs.gov/cch/dsas), an ArcGIS software extension that calculates historical shoreline change metrics, including End Point Rate (EPR) and Linear Regression Rate. The EPR, widely used for analyzing shoreline changes, reflects the movement rate of boundary between the earliest and most recent observations. Regions with natural-significant alterations and well-defined boundaries were chosen for detailed change analysis. The vegetation boundary was defined as the interface between the mudflat and vegetation, and the mudflat boundary was characterized as the interface between water and mudflat (Fig. 1A). Boundaries were extracted from the GEE-classified results and manually outlined to ensure accuracy and continuity (Fig. 2A, B). All shoreline vectors were projected to WGS 1984 UTM Zone 49 N with the WGS 1984 datum before DSAS analysis. For the DSAS analysis, a baseline was established approximately parallel to the shoreline (Fig. 2C, D). Transects were generated perpendicular to the baseline, extending from the baseline toward the lakeward limit of the shoreline, with an interval of 100 m between adjacent transects (Fig. 2C, D). Specific transects number and average length by subregions were shown in Table S5. Subsequently, DSAS was employed to calculate the boundary change rate:

$$EPR = \frac{\Delta D}{\Delta Y} \quad (1)$$

Where ΔD represents the distance in meters between two boundary lines; ΔY represents the time elapsed between the oldest and most recent measurements. For each subregion, the expansion rate was calculated by averaging the EPR values along all transects, and the mean was reported together with its standard deviation (Table S5).

This study introduces a novel framework that integrates GEE-based classification with DSAS shoreline analysis to map multi-decadal wetland vegetation dynamics and quantify boundary migration across DTL (Fig. S4). Leveraging open-access satellite archives, the approach is both robust and replicable, offering broad applicability to other river-connected lakes. In the following sections, we present results linking vegetation dynamics to long-term changes in inflow and sediment load, and further discuss the mechanisms driving wetland evolution.

3. Results

3.1. DTL hydrological dynamics

Over the past 30 years, the hydrological parameters of DTL presented distinct variations (Fig. 3). Specifically, the Three Inlets and Four Waters, two groups of inflow tributaries, exhibited varying degrees of decline in both water flow and SSD (Fig. 3A, D). The Three Inlets decreased in flow from $62.47 \pm 17.12 \times 10^9$ m^3 to $47.04 \pm 16.73 \times 10^9$ m^3, along with a sharp reduction in SSD from $66.83 \pm 33.19 \times 10^6$ t to $7.12 \pm 34.63 \times 10^6$ t, representing a decline of nearly 90%. Similarly, the Four Waters experienced a decrease in flow from $181.96 \pm 24.19 \times 10^9$ m^3 to $161.99 \pm 24.72 \times 10^9$ m^3 and sediment load from $19.52 \pm 6.80 \times 10^6$ t to $6.96 \pm 7.06 \times 10^6$ t. Overall, the total inflow dropped from $244.43 \pm 28.71 \times 10^9$ m^3 to $209.03 \pm 29.67 \times 10^9$ m^3, and the total sediment input dropped from $86.36 \pm 4.65 \times 10^6$ t to $14.09 \pm 5.18 \times 10^6$ t, suggesting an overall reduction of approximately 84% (Fig. 3B, E).

In terms of lake outflow, both water discharge and sediment load at the Chenglingji station exhibited stage-wise declines. The average discharge decreased from $281.83 \pm 41.82 \times 10^9$ m^3 to $242.13 \pm 42.22 \times 10^9$ m^3, while the sediment output dropped from $24.57 \pm 36.06 \times 10^6$ t to $16.75 \pm 38.20 \times 10^6$ t (Fig. 3B, E). From the perspective of net change, although the lake maintained a state of net outflow, the magnitude of net discharge decreased (in absolute value) from $-37.40 \pm 15.01 \times 10^9$ m^3 to $-33.10 \pm 14.61 \times 10^9$ m^3 (Fig. 3C). In contrast, the net sediment flux (inflow minus outflow) dropped sharply (Fig. 3F). Notably, the net sediment budget turned negative after 2006, with the average value decreasing from $61.79 \pm 33.76 \times 10^6$ t to $-2.67 \pm 35.16 \times 10^6$ t (Fig. 3F).

The annual average water level at Chenglingji station showed an obvious downward trend from 1989 to 2023, declining from 25.49 ±

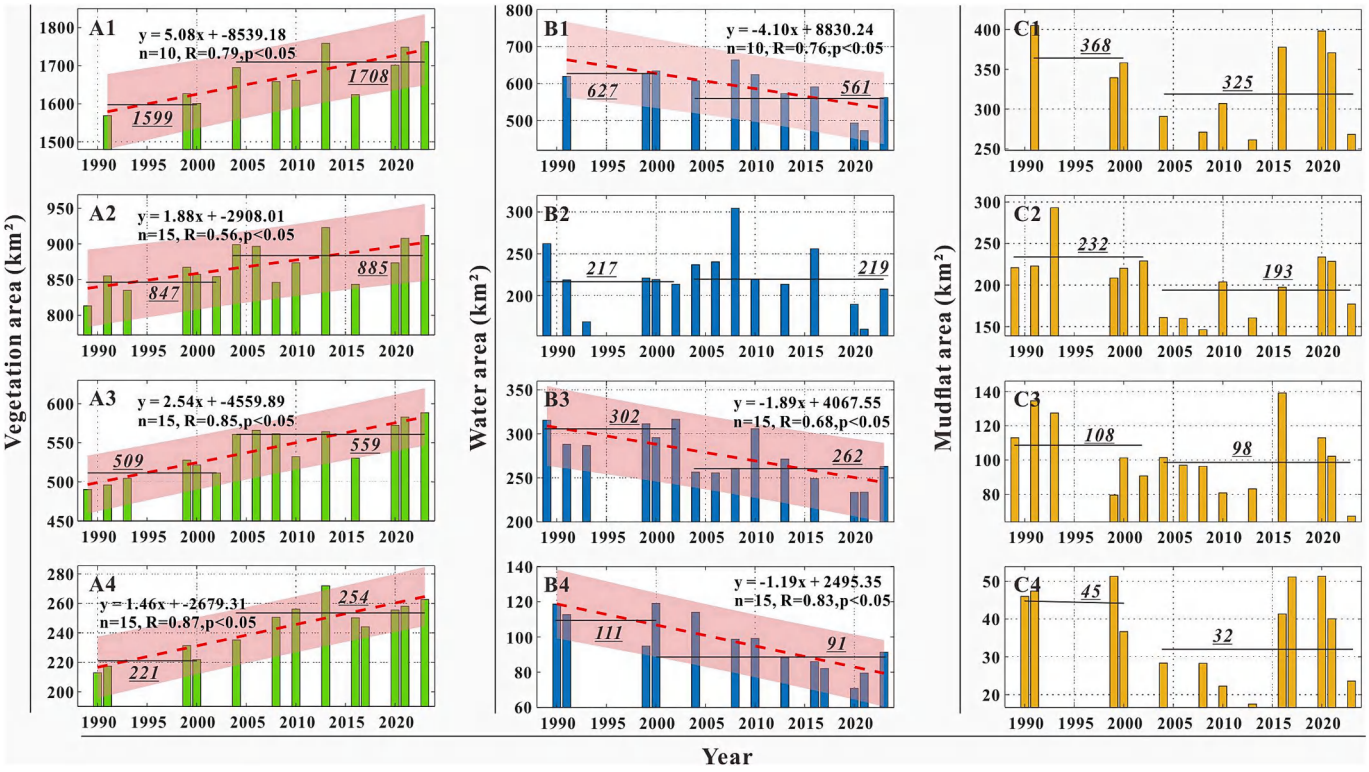

Fig. 4. Area change of vegetation (A1-A4), water body (B1-B4), and mudflat (C1-C4) in entire DTL and its subregions from 1989 to 2023. Panels 1–4 correspond to the entire DTL, East DTL, South DTL, and West DTL, respectively.

0.51 m before 2003 to 24.87 ± 0.51 m after 2003 (a reduction of approximately 0.6 m) (Fig. 3G). Monthly average water levels were consistently lower during the post-TGD period, particularly between July and October (Fig. 3K). Concurrent with the water level decrease, the duration of dry season in DTL lengthened by 35 days, extending from 158 ± 34 days to 193 ± 34 days (Fig. 3H). Specifically, this extension was mainly reflected in the dry season starting 27 days earlier and ending 8 days later (Fig. 3I, J). Compared with the pre-TGD period, the water level-discharge curve during the post-TGD period exhibited only a slight change in trend, characterized by marginally higher water levels at low discharges and slightly lower water levels at high discharges (Fig. 3L).

3.2. Vegetation area trends

Over the past three decades, the wetland vegetation area of DTL as a whole, along with its three subregions (East, South, and West), exhibited a consistent increasing trend, differing only in the rate of change. For the entire DTL, the wetland vegetation expanded significantly at a rate of 5.08 km^2/yr, increasing from 1599 ± 29 km^2 before 2003 to 1709 ± 52 km^2 after 2003 (Fig. 4A1), accompanied by a significant decrease in water area at a rate of 4.10 km^2/yr (Fig. 4C1). In contrast, the mudflat area exhibited fluctuation over time without a discernible trend (Fig. 4B1).

Among the subregions, the vegetation area of East DTL increased at a rate of 1.88 km^2/yr, growing from 813 km^2 in 1989 to 912 km^2 in 2023. When examined in two phases, the vegetation expanded from 847 ± 20 km^2 (pre-2003) to 885 ± 28 km^2 (post-2003), indicating a slight deceleration in the later phase (Fig. 4A2). Meanwhile, the water and mudflat areas remained relatively stable (Fig. 4B2, C2). In South DTL, vegetation expansion occurred at a rate of 2.54 km^2/yr, which was closely linked to a simultaneous decline in water area at a rate of 1.89 km^2/yr (Fig. 4A3, B3). A similar pattern was observed in West DTL, where vegetation grew at a rate of 1.46 km^2/yr, while the water area shrank at a rate of 1.19 km^2/yr (Fig. 4A4, B4).

3.3. Spatial patterns of gain and loss

Over the past few decades, wetland vegetation in all three subregions of DTL gradually expanded lakeward, at varying magnitudes (Fig. 5). In East DTL, vegetation coverage increased from 62% in 1989 to 70% in 2023, with approximately 158 km^2 of new vegetation emerging along the vegetation edges, notably in Zone 1 and Zone 2, while vegetation loss were concentrated in Zone 3 since 2013, amounting to about 60 km^2 (Fig. 5A, Fig. 6A1, B1).

In South DTL, vegetation coverage rose from 53% in 1989 to 64% in 2023, with the central area transitioning from fragmented to continuous patches (Zone 4), accompanied by substantial vegetation expansion in Zone 5 and Zone 6, although localized irregular patches of vegetation loss occurred near the mouth of the Zi River (Fig. 5B, Fig. 6A2). Quantitatively, the net vegetation gain and loss during 1989–2023 were approximately 140 km^2 and 42 km^2, respectively. In West DTL, vegetation coverage underwent the most significant change, increasing from 56% in 1991 to 69% in 2023. Zone 7, previously dominated by non-vegetated areas in 1991, gained around 67 km^2 of new vegetation by 2023 (Fig. 5C, Fig. 6A3). In addition, patchy vegetation loss appeared in both the southern (Zone 8, 1991–2000) and northern West DTL, totaling about 17 km^2 (Fig. 6A3; Fig. 6B3).

3.4. Boundary-change rates

In DTL, vegetation, mudflats, and water bodies are sequentially distributed along a decreasing elevation gradient, indicating that vegetation expansion is influenced and constrained by the extent of mudflat and water bodies. In East DTL, typical vegetation transects expanded lakeward at an average rate of about 27.56 ± 27.03 m/yr from 1989 to 2023, ranging from −14 m/yr to 102 m/yr (Fig. 6C1; Table S5). The highest expansion rate of 102 m/yr, observed near the mouth of the

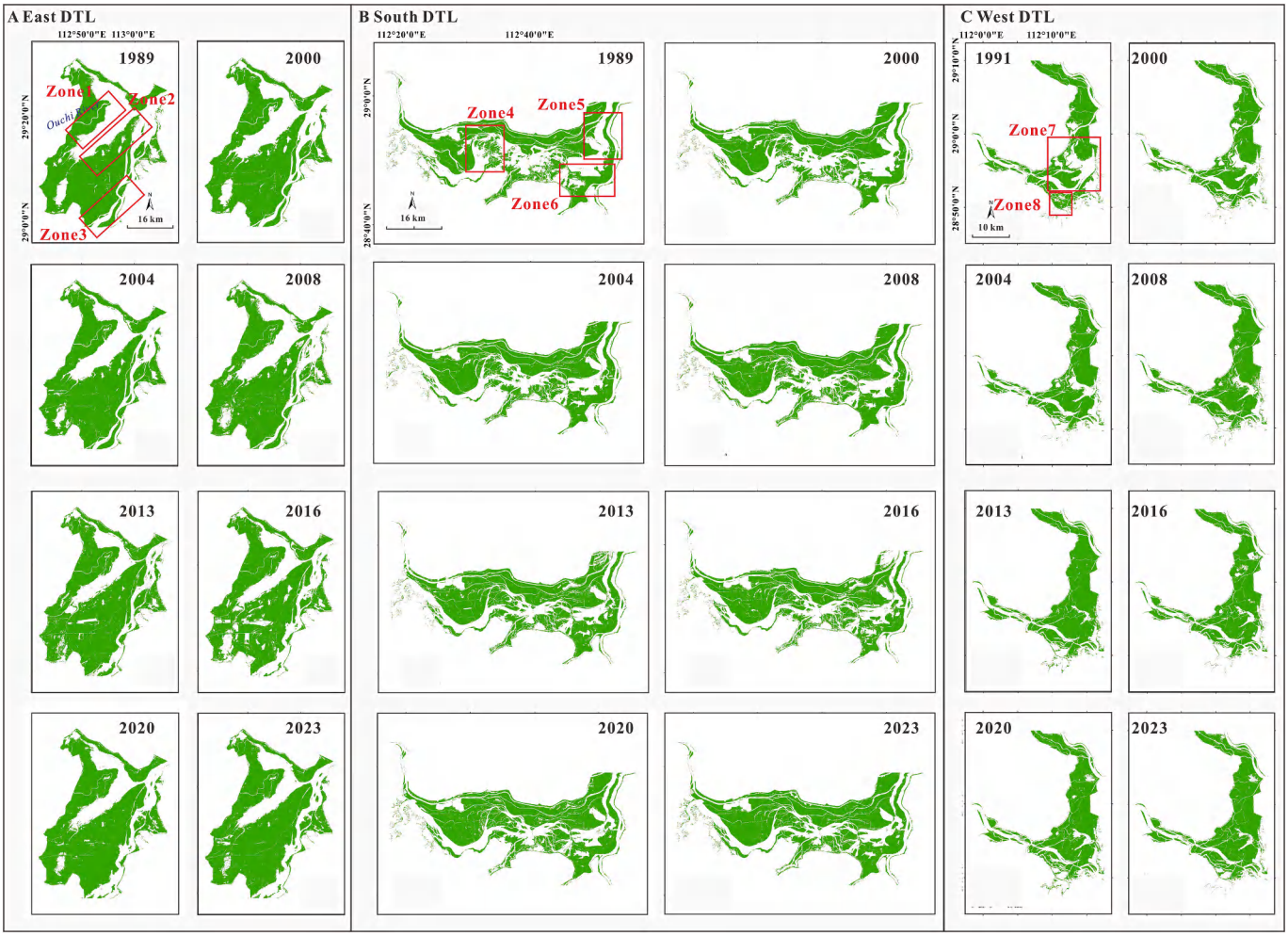

Fig. 5. Spatial distribution of wetland vegetation at subregions: A. East DTL; B South DTL; C. West DTL. Each panel shows vegetation for multiple years, with red boxes highlighting areas with notable changes. (For interpretation of the references to colour in this figure legend, the reader is referred to the web version of this article.)

Ouchi River, was accompanied by the most rapid progradation of the mudflat boundary at a rate of 73 m/yr (Fig. 2A1, B1). Meanwhile, the mudflat boundary advanced toward the lake center at an average rate of approximately 10.51 ± 15.82 m/yr, ranging from −55.52 m/yr to 88.09 m/yr, with retreat being observed in only a small number of transects (Fig. 2E1).

In South DTL, the expansion of vegetation boundary was consistent with its spatial changes, with most of the shoreline expanding at an average rate of 13.74 ± 14.45 m/yr, varying from −18.05 m/yr to 72.43 m/yr (Fig. 6C2). Pronounced mudflat boundary changes mainly occurred near the Xiang River mouth, with an average rate of 18.30 ± 22.04 m/yr, ranging from −7.50 m/yr to 70.08 m/y (Fig. 2E2). In West DTL, all typical vegetation transects advanced toward the lake center at an average rate of 22.45 ± 20.67 m/yr (Fig. 6C3). The mudflat boundary also exhibited expansion, at an average rate of 8.50 ± 8.35 m/yr between 1991 and 2023, ranging from −4.25 m/yr to 33.32 m/yr (Fig. 2E3).

4. Discussion

4.1. Role of precipitation and temperature

Climate factors, including precipitation and temperature, are crucial for lake wetland ecosystems (Jiang et al., 2011; Zhang et al., 2021; Yao et al., 2022). Previous studies have reported a prominent correlation between the vegetation index and precipitation in terms of spatial distribution (Jiang et al., 2011), while temperature has also been shown to substantially influence vegetation growth by regulating photosynthesis and extending the growing season (Yin et al., 2024). In the DTL basin, long-term observations showed little variation in annual precipitation but a significant increasing in temperature (Fig. 7). Correlation analysis further indicated a significant positive relationship between temperature and vegetation area, suggesting that rising temperature promotes vegetation growth (Fig. S3). In contrast, the weak and negative relationship between vegetation area and precipitation may be attributed to the indirect role (Fig. S3), as precipitation primarily affects vegetation through regulating environmental moisture conditions (Zhang et al., 2021). Collectively, these results suggested that although both precipitation and temperature are important climatic drivers, their direct contributions to vegetation dynamics appear limited, consistenting with the findings of Zhang et al. (2021). Instead, hydrological alterations and other non-climatic factors may play a more decisive role in shaping vegetation changes.

4.2. Effects of hydrological alteration

Hydrological alterations, induced by operation of the TGD and other basin-wide reservoirs, played a pivotal role in driving the observed wetland vegetation expansion in DTL (Fig. 8A). These alterations shifted the lake from a net depositional to a net erosional phase, leading to

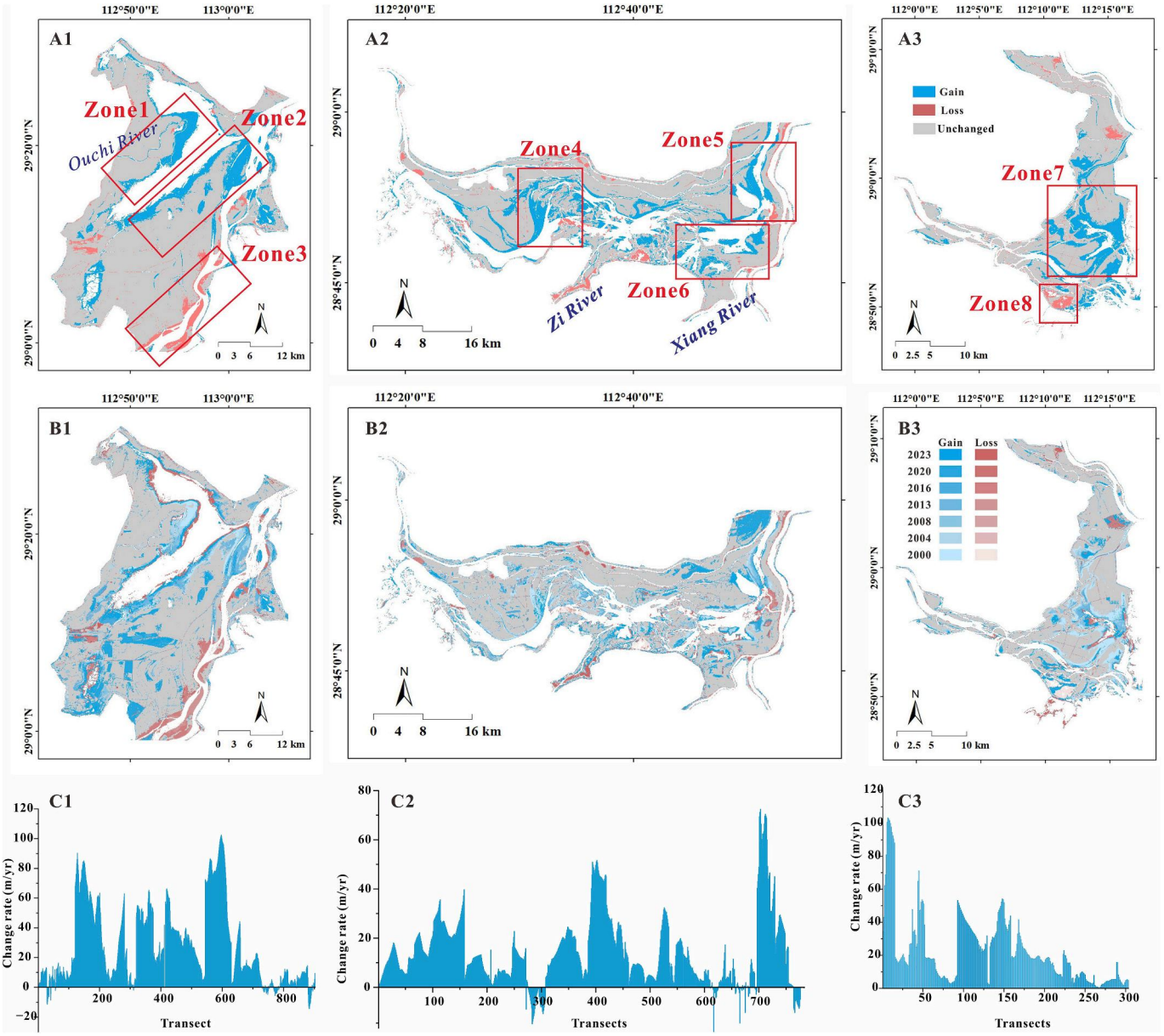

Fig. 6. Gain and loss of vegetation and change rate of vegetation boundary in East, South, and West DTL. A. Total gain and loss from 1989 to 2023; B. Gain and loss for each 4-year interval (specific years and changes shown in the legend); C. Change rate of vegetation boundaries along transects. Panels 1–3 correspond to the East DTL, South DTL, and West DTL, respectively.

intensified channel and lakebed scouring, as confirmed by cross-sectional changes at the Chenglingji and Nanzui transects (Fig. 8B, C). Sustained scouring deepened the lakebed and contributed to a long-term decline in lake water levels, which in turn caused earlier exposure of the lakebed and extended the duration of the dry season (Fig. 3G-J). These changes represent key factors regulating vegetation dynamics in lacustrine wetlands (Xie et al., 2014; Liu et al., 2024).

The negative correlation between vegetation area and water level, together with the positive correlation with the duration of the dry season (Fig. S3), indicated that vegetation expansion was promoted by both declining lake water levels and prolonged dry periods. Lower water levels exposed more lakebeds, while the contraction of open water leaded to waterline retreat and the exposure of previously submerged mudflats. Meanwhile, the earlier onset and longer duration of the dry season created favorable temporal windows for vegetation establishment by improving soil aeration and reducing submersion stress (Hu et al., 2018; Yang et al., 2020). Field observations and remote sensing analyses confirm that such conditions facilitated the rapid colonization by pioneer species, primarily *Carex* spp., and promoted a downward shift in the lower elevation boundary of vegetation (Gao et al., 2020; Mu et al., 2020). Under these combined effects, newly formed substrates were rapidly colonized by wetland vegetation, forming a spatial transition zone from water to mudflat to vegetated land—a classic trajectory of wetland development under hydrological stress (Xie et al., 2014). Quantitative assessments in DTL revealed clear evidence of this process: during the dry season, approximately 120.83 km^2, 91.32 km^2, and 43.19 km^2 of water area retreated in the East, South, and West subregions, respectively, while nearly equivalent areas of mudflat (118.17 km^2, 88.38 km^2, and 40.30 km^2) were subsequently colonized by vegetation (Fig. 9).

While Hu et al. (2018) identified submergence condition as the primary driver of vegetation distribution in East DTL up to 2015, our study extended this understanding by incorporating an additional six years of data, expanding the analysis to the southern and western subregions,

and explicitly considering multiple synergistic drivers, including precipitation, water level, and dry season duration (Table S8). Under this framework, vegetation dynamics in different subregions of DTL exhibited distinct responses: vegetation expansion in East DTL was primarily controlled by declining water levels, followed by the duration of the dry season, while precipitation played a comparatively minor role. In contrast, vegetation dynamics in the South and West DTL were most strongly influenced by the duration of dry season, with secondary contributions from precipitation and water level changes.

Similar patterns have also been observed in Poyang Lake, another Changjiang River-connected freshwater lake, where hydrological alterations from the TGD and regional reservoirs have driven substantial lakeward expansion of wetland vegetation (Mu et al., 2020; Mei et al., 2016; Bu et al., 2025), underscores the profound influence of river regulation on river-lake ecosystems. Collectively, the extended exposure of lakebed provided the temporal window for plant colonization, while the decrease in water level created the physical space for plant expansion, jointly reinforcing vegetation growth under sustained hydrological stress.

4.3. Vegetation–sediment feedback mechanisms

Sediment input represents a fundamental material source for wetland vegetation expansion. From 1989 to 2023, sediment input to the subregions of DTL exhibited a marked decline, with the year 2003 being identified as a turning point. Specifically, mean annual sediment loads to the eastern, southern, and western subregions decreased from $21.36 \pm 12.93 \times 10^6$ t, $9.21 \pm 3.91 \times 10^6$ t, and $55.79 \pm 23.78 \times 10^6$ t, respectively, to $2.24 \pm 2.10 \times 10^6$ t, $4.92 \pm 3.01 \times 10^6$ t, and $7.03 \pm 4.90 \times 10^6$ t (Fig. 10A-C). Correlation analysis between sediment input and the mean rate of shoreline expansion during each stage revealed a significant positive relationship across all subregions, highlighting the critical role of sediment supply in facilitating lakeward vegetation growth (Fig. 10D). Sedimentation rates varied spatially due to hydrodynamic differences, with mean annual mass accumulation rates of 1.52 g cm^{-2} yr^{-1}, 1.21 g cm^{-2} yr^{-1}, and 0.89 g cm^{-2} yr^{-1} in the West, South, and East DTL, respectively (Chen et al., 2025). However, vegetation expansion did not directly follow these rates: the eastern subregion, despite having the lowest accumulation rate, exhibited the fastest lakeward advance, suggesting that hydrodynamic disturbances and hydrological alterations modulated the effect of sediment supply on vegetation expansion.

Furthermore, vegetation interacts with sediment dynamics, forming a self-reinforcing feedback loop that enhances its own growth and expansion. Plant roots and stems reduce flow velocity and turbulent kinetic energy, effectively trap suspended sediments, enhance sediment deposition, and contribute to bed elevation gain (Zhang et al., 2020; Peng et al., 2022). The trapped organic-rich deposits further improve substrate conditions and nutrient availability, facilitating plant establishment and growth (Clarke and Wharton, 2001). During the rising-water period, vegetation effectively captures suspended sediments by reducing flow velocity, thereby promoting substantial deposition and accelerating bed elevation gain. This mechanism is supported by Zhang et al. (2020), who reported that the presence of vegetation increased sediment deposition thickness over one flood season by up to 190% compared with bare bed.

During the falling-water period, sediments gradually consolidate while root systems further stabilize these deposits, effectively protecting the elevated surface from erosion. In the subsequent dry season, this vegetation-driven elevation gain allows mudflats to emerge earlier as water level falls, reducing submergence duration and improving drainage conditions, which together create favorable environments for vegetation growth. With the further drop of water levels in the following dry season, more extensive mudflats are exposed, providing additional space for vegetation expansion (Fig. 11B). These conditions collectively promote denser vegetation establishment and, in the subsequent hydrological cycle, substantially enhance sediment-trapping capacity, thereby reinforcing the self-sustaining feedback between vegetation growth and sediment accretion. This feedback process is further corroborated by significant vegetation expansion observed in low-elevation littoral zones (Fig. 6A, B), consistent with previous findings (Zhang et al., 2021; Cai et al., 2020; Gao et al., 2020).

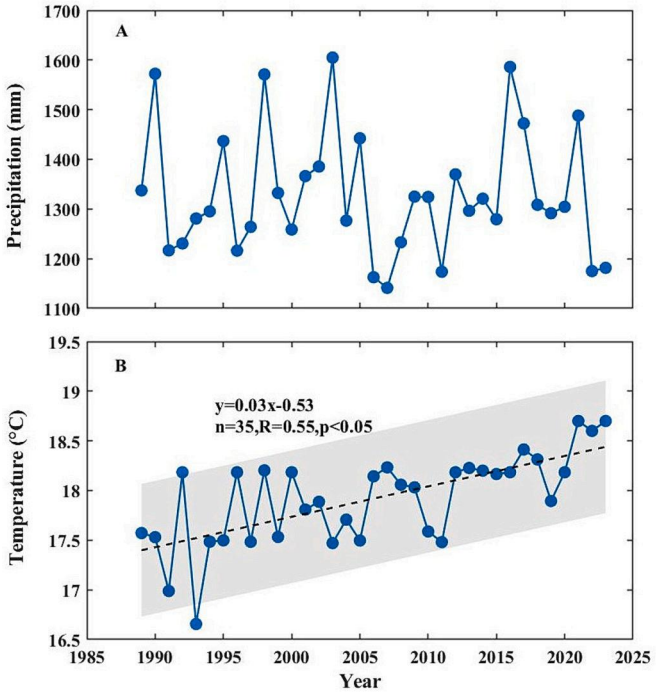

Fig. 7. Basin-wide Annual precipitation (A)and temperature (B).

In summary, the vegetation-sediment feedback establishes a self-reinforcing cycle: fluvial sediment delivery supplies the material for colonization, bed elevation gain enables plant establishment, which, in turn, accelerates further sediment accumulation (Fig. 11A). This process progressively reduces open-water areas and constitutes a key driver of ongoing lake shrinkage.

4.4. Impacts of human activities within lake

Local activities within the lake, including reclamation and sand mining, have significantly impacted the wetlands of DTL, causing direct vegetation loss and bed degradation (Zheng et al., 2022). From 1989 to 2023, approximately 32.0 km^2, 8.8 km^2, and 11.2 km^2 of mudflat and vegetation were reclaimed into water bodies (e.g., ponds) in the East, South, and West DTL, respectively (Fig. 12A-C, D3). Sand mining, concentrated in East (45.9 km^2) and South DTL (19.8 km^2), directly led to patchy vegetation loss, including 3.86 km^2 in the channel of the Zi River during 2020–2023 (Fig. 6B2, Fig. 12A-D). Notably, no sand mining was detected throughout 2017–2020, consistent with the suspension of commercial mining in the lake because of a strict government ban (People' s Government of Hunan Province, 2017; Han et al., 2023). In summary, reclamation and sand mining have led to substantial and predominantly long-term vegetation loss in DTL, with a total of over 52.0 km^2 of vegetated land converted and more than 65.7 km^2 directly affected by sand mining. Furthermore, other anthropogenic pressures such as dredging, aquaculture, and downstream withdrawals may also substantially influence wetland morphology.

Taken together, our findings can be synthesized into the following conceptual model of wetland evolution in DTL (Fig.11): (a) Climatic variability, including rainfall fluctuations and rising temperatures, regulates water supply and vegetation growth. (b) TGD operations lower lake water levels and prolong lakebed exposure, facilitating vegetation

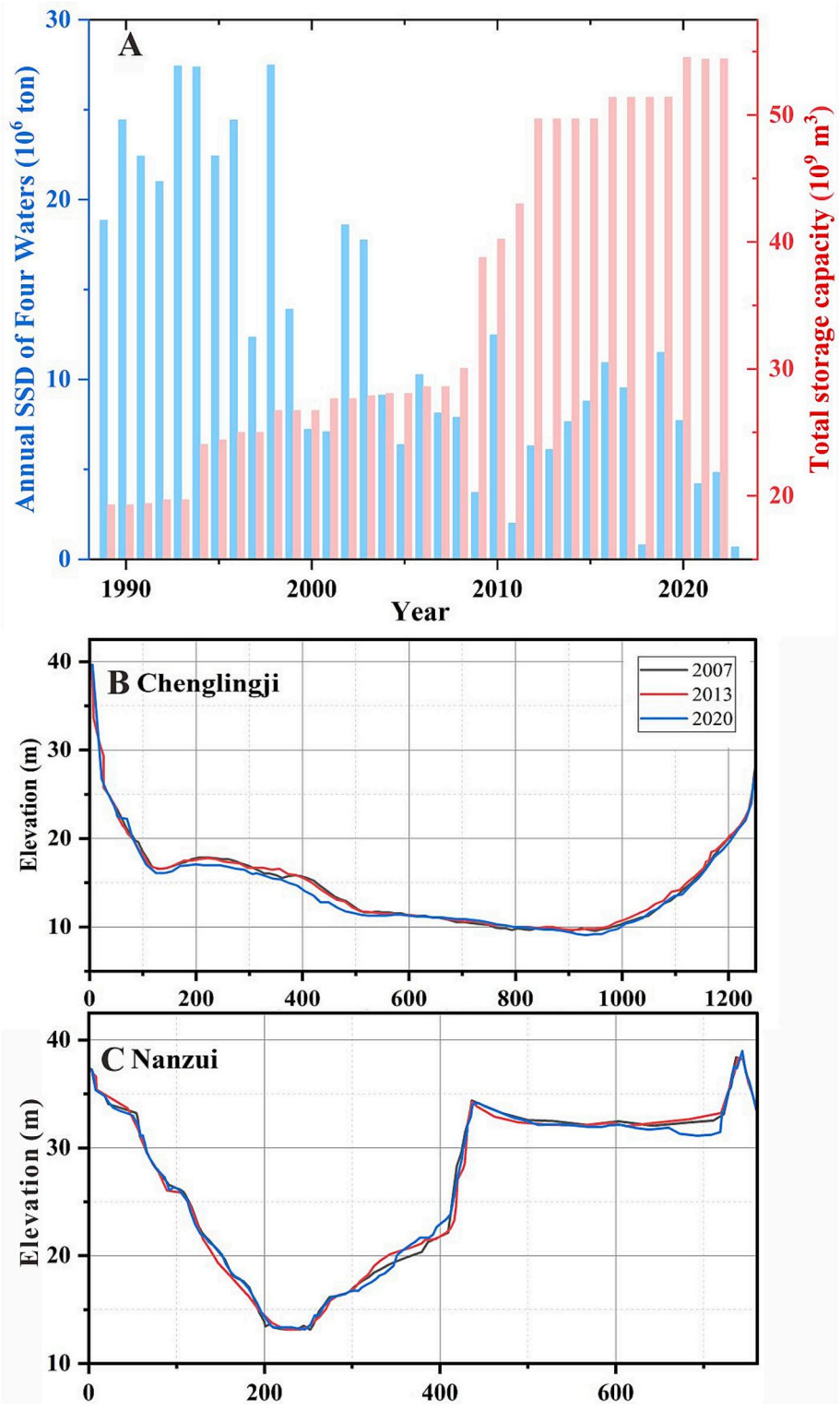

Fig. 8. A. Annual SSD of Four Water and the cumulative capacity of more than 14,000 reservoirs in the DTL basin; B—C. Elevation change of transect at Chenglingji and Nanzui.

colonization. (c) Vegetation enhances sediment trapping despite declining sediment input, creating a positive feedback loop that promotes its expansion and stabilizes mudflats. (d) Human activities, such as reclamation and sand mining, cause localized vegetation loss. (e) The synergy of these climatic, hydrological, sedimentary, and anthropogenic processes collectively drives water area shrinkage and the progressive lakeward expansion of mudflats and vegetation. This integrated hydro-sediment-vegetation framework provides a novel perspective on wetland evolution.

Under the combined influence of natural and anthropogenic factors, advanced phenology and extended dry-season duration of wetland vegetation have substantially altered the ecosystem structure and function of DTL. While increased vegetation coverage benefits some waterbirds, earlier growth and senescence reduce meadow quality and

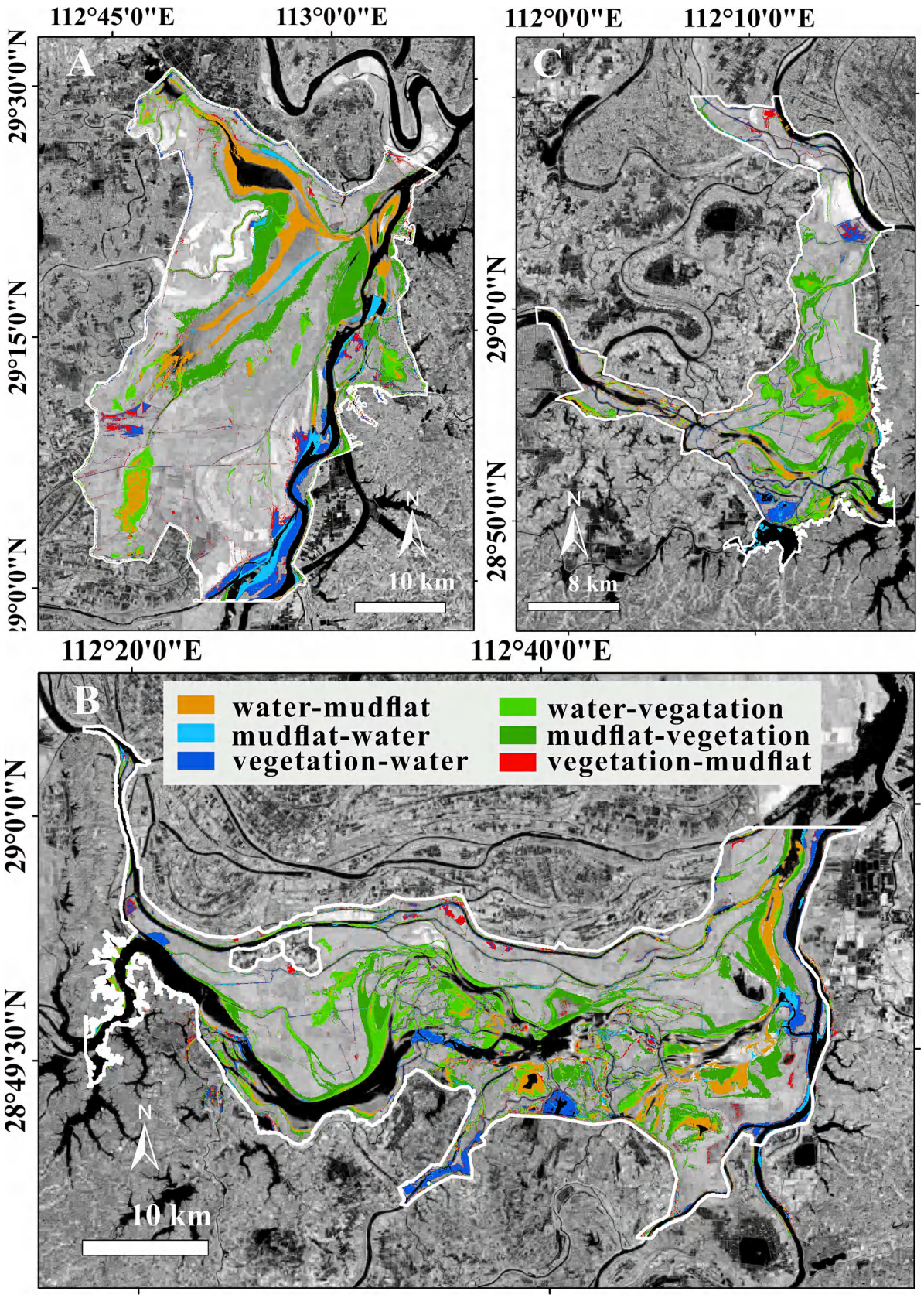

Fig. 9. Transition of different landcover at: A. East DTL; B. South DTL; C. West DTL.

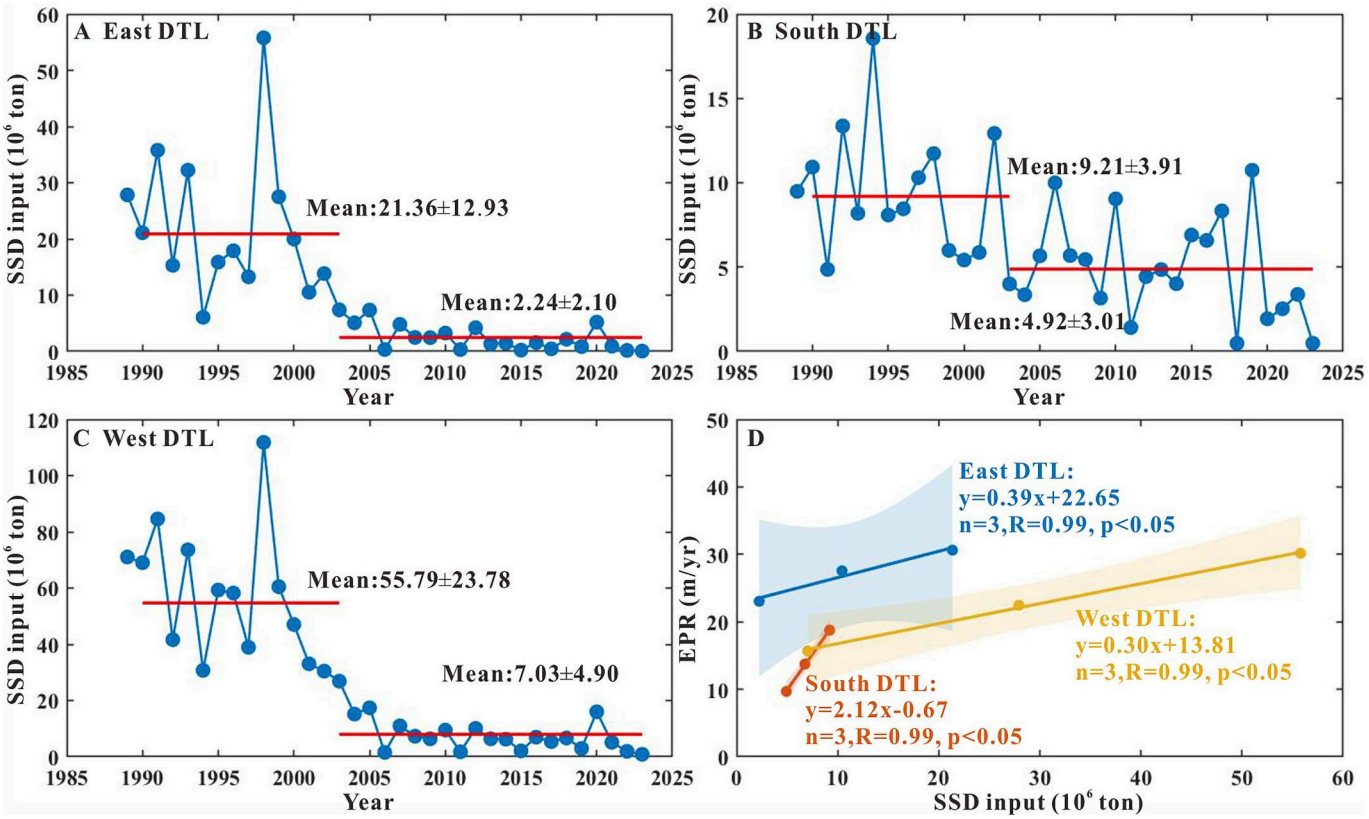

Fig. 10. Sediment input of DTL sub-regions: (A) East, (B) South, (C) West; (D) correlation between the stage-wise mean sediment input in each sub-region and the average expansion rate of wetland vegetation boundary.

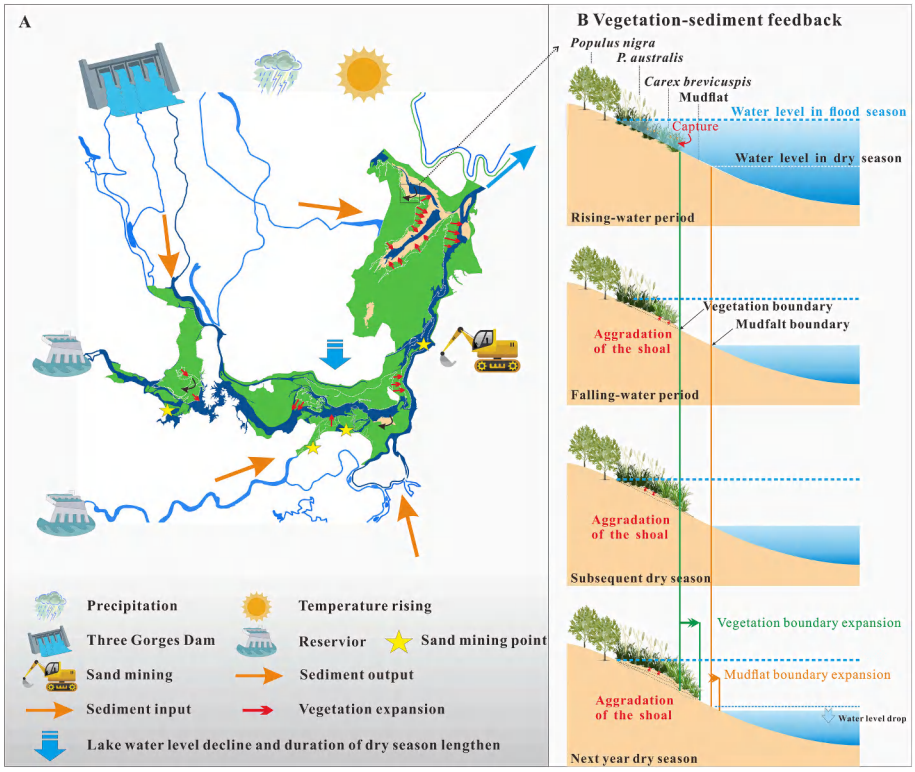

Fig. 11. A. Conceptual model of wetland evolution in DTL. B. Mechanism of vegetation-sediment feedback.

misalign feeding windows for herbivorous migratory birds, particularly geese. To mitigate these ecological impacts, basin-scale water regulation

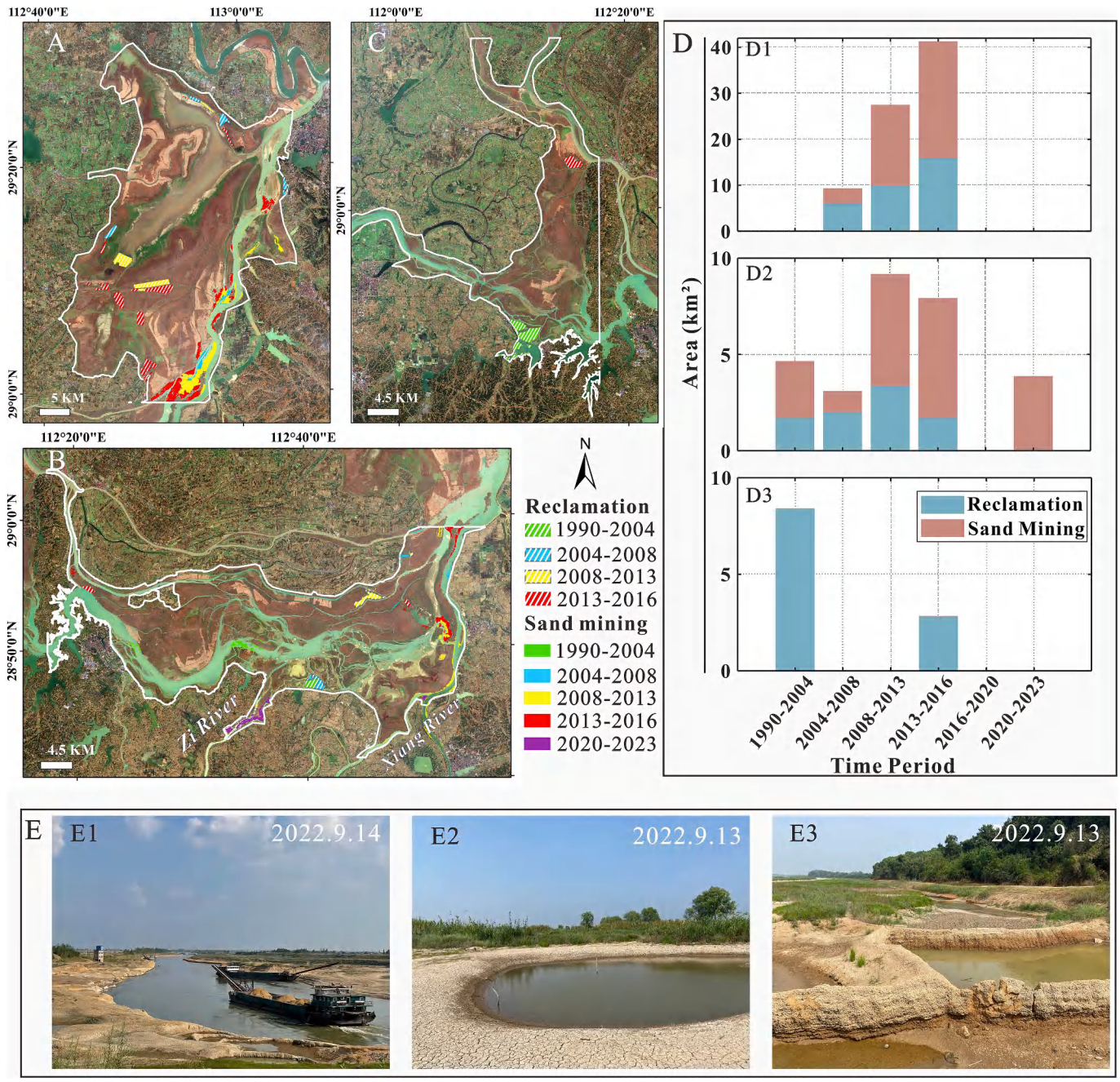

Fig. 12. Reclamation and sand mining distribution at A. East DTL; B. South DTL; C. West DTL; D. Area of reclamation and sand mining at East DTL(D1), South DTL (D2), West DTL (D3); E. human activities (photos taken on 13–14 Sep., 2022).

should be optimized to align water levels with vegetation phenology and migratory bird cycles. In addition, strict controls on sand mining and reclamation are necessary to prevent further vegetation loss and lakebed degradation, thereby maintaining wetland stability and biodiversity.

4.5. Limitations and future directions

Despite the robustness of our dataset and analyses, several limitations warrant acknowledged. Differences in sensor characteristics and revisit cycles between Landsat (30 m) and Sentinel-2 (10 m) may introduce inconsistencies in classification accuracy or vegetation detection. Class-specific errors, spatial heterogeneity in misclassification, and mixed pixels can lead to over- or underestimation of wetland vegetation, as the random forest algorithm operates on a per-pixel basis. Despite high classification accuracy (overall >88%, PA/UA >85%), interannual vegetation area estimates may exhibit uncertainties of up to ±247.5 km^2/yr due to persistent misclassification errors. Although dry-season imagery at similar water levels was used to minimize the influence of inundation, interannual fluctuations in water level may still introduce bias into the classification results and the apparent extent of vegetation gains.

In addition, the absence of in-situ measurements of floodplain elevation changes prevented direct assessment of sediment accretion. While previous studies suggest that vegetation enhances sediment trapping, which support our proposed vegetation–sediment feedback mechanism (Zhang et al., 2020; Peng et al., 2022), field monitoring of bed-level changes would provide essential empirical validation. Additionally, this study lack a fully account of other potential drivers that

may affect the dynamics of vegetation and sediments, such as solar radiation, drought, and flood. Future research should incorporate these factors, along with field-based monitoring and higher-resolution data, to achieve a more comprehensive understanding of wetland evolution.

5. Conclusion

As a vital wetland ecosystem in China, DTL wetland holds immense ecological and economic significance. However, its vegetation faces strong pressure from hydrological alterations driven by both natural processes and human activities. Herein, we analyzed long-term vegetation dynamics in DTL using high-resolution remote sensing images and assessed the relative contributions of driving factors. The main conclusions are summarized as follows:

(1) From 1989 to 2023, the hydrological conditions of DTL changed markedly, strongly associated with the regulation of TGD since 2003. A sharp decline in sediment inflow shifted the sediment budget from positive to negative, indicating a transition in the sedimentation pattern from net accumulation to net erosion. Meanwhile, the annual mean water level at Chenglingji dropped by approximately 0.6 m, and the dry season lengthened by about 35 days, starting 27 days earlier and ending 8 days later.

(2) The wetland vegetation area of DTL increased overall at a rate of 5.08 km^2/yr, with subregional rates of 1.88 km^2/yr (East), 2.54 km^2/yr (South), and 1.46 km^2/yr (West). Vegetation in all subregions expanded lakeward, characterized by significant expansion in the central East and West DTL, and the merging of fragmented into continuous patches in South DTL, although irregular local losses also occurred. Shoreline analysis further shows predominant lakeward expansion at average rates of 27.56 $\pm$ 27.03 m/yr (East), 13.74 $\pm$ 14.45 m/yr (South), and 22.45 $\pm$ 20.67 m/yr (West), with a few transects showing retreat.

(3) Hydrological alterations, particularly declining water level and prolonged dry season driven by the operation of TGD, have strongly influenced wetland dynamics. Vegetation area showed a negative correlation with water level and a positive correlation with dry season duration, with distinct subregional responses: East DTL was mainly regulated by water level decline, whereas South and West DTL were more sensitive to dry season duration.

(4) Sediment input provides material for vegetation expansion, while the vegetation-sediment feedback further accelerates wetland evolution by reducing flow velocity, trapping suspended sediments, and raising floodplains elevation. Furthermore, reclamation and sand mining have caused long-term impacts by converting 52.0 km^2 of wetlands into ponds and removing 65.7 km^2 in East and South DTL, which offsets the natural expansion processes at a local scale.

CRediT authorship contribution statement

Jiangjie Yang: Writing – original draft, Visualization, Formal analysis, Data curation. **Zhijun Dai:** Writing – review & editing, Writing – original draft, Supervision, Methodology, Funding acquisition, Formal analysis, Data curation, Conceptualization. **Xuefei Mei:** Writing – review & editing, Supervision, Methodology. **Fangyuan Bu:** Formal analysis, Data curation. **Yizhuang Liu:** Methodology, Formal analysis.

Declaration of competing interest

The authors declare that they have no known competing financial interests or personal relationships that could have appeared to influence the work reported in this paper.

Acknowledgements

This research was supported by the National Natural Science Key Foundation of China (42430406), the National Social Science Foundation Major Project of China (23&ZD105), and the National Natural Science Foundation of China (42576163).

Appendix A. Supplementary data

Supplementary data to this article can be found online at https://doi.org/10.1016/j.catena.2026.109821.

Data availability

Landsat5/7/8/9 and Sentinel-2 (Original data) (U.S. Geological Survey (USGS))

References

Arono, S., 1985. The minimum accuracy value as an index of classification accuracy. Photogramm. Eng. Remote. Sens. 51 (1), 99–111.
Asselen, S.V., Verburg, P.H., Vermaat, J.E., Janse, J.H., 2013. Drivers of wetland conversion: a global meta-analysis. PloS One 8 (11), e81292.
Bu, F.Y., Dai, Z.J., Mei, X.F., Chu, A., Cheng, J., Lan, L., 2025. Machine learning-based mapping wetland dynamics of the largest freshwater lake in China. Global Ecology and Conservation 59, e03585.
Cai, Y., Liu, S., Lin, H., 2020. Monitoring the vegetation dynamics in the Dongting Lake wetland from 2000 to 2019 using the BEAST algorithm based on dense Landsat time series. Appl. Sci. 10, 4209. https://doi.org/10.3390/app10124209.
Chen, M., Peng, A., Wu, M., Li, X., He, H., 2025. Comparisons of sediment mass accumulation rates in different regions of Dongting Lake and their environmental indications: based on $^{239+240}$Pu, ^{137}Cs, and ^{210}Pbex. J. Environ. Radioact. 287, 107702. https://doi.org/10.1016/j.jenvrad.2025.107702.
Clarke, S.J., Wharton, G., 2001. Sediment nutrient characteristics and aquatic macrophytes in lowland English rivers. Sci. Total Environ. 266 (1–3), 103–112. https://doi.org/10.1016/s0048-9697(00)00754-3 (PMID: 11258806).
Congalton, R.G., 1991. A review of assessing the accuracy of classifications of remotely sensed data. Remote Sens. Environ. 37, 35–46. https://doi.org/10.1016/0034-4257(91)90048-B.
Davidson, N., 2014. How much wetland has the world lost? Long-term and recent trends in global wetland area. Mar. Freshw. Res. 65 (10), 934–941.
Deng, F., Wang, X., Cai, X., et al., 2014. Analysis of the relationship between inundation frequency and wetland vegetation in Dongting Lake using remote sensing data. Ecohydrology 7 (2), 717–726.
Gao, Y., Xie, Y., Zou, D., 2020. Hydrological regime change and its ecological responses in east Dongting Lake, China. Ecohydrol. Hydrobiol. 20, 142–150.
Gehring, T.M., Blass, C.R., Murry, B.A., Uzarski, D.G., 2020. Great Lakes coastal wetlands as suitable habitat for invasive mute swans in Michigan. J. Gt. Lakes Res. 46 (2), 323–329.
Gorelick, N., Hancher, M., Dixon, M., Ilyushchenko, S., Thau, D., Moore, R., 2017. Google earth engine: planetary-scale geospatial analysis for everyone. Remote Sens. Environ. 202, 18–27.
Grove, A.T., 1996. African river discharges and lake levels in the twentieth century. In: Odada, T.C. Johnson amd E. (Ed.), The Limnology, Climatology, and Palaeoclimatology of the East African Lakes. N.J, Gordon and Breach, Newark, pp. 95–100.
Guo, D., Shi, W., Qian, F., Wang, S., Cai, C., 2022. Monitoring the spatiotemporal change of Dongting Lake wetland by integrating Landsat and MODIS images, from 2001 to 2020. Ecol. Informatics 72, 101848.
Han, Q., Zhang, S., Huang, G., Zhang, R., 2016. Analysis of long-term water level variation in Dongting Lake. China. Water 8 (7), 1–21.
Han, Y., Xu, W., Liu, J., Zhang, X., Wang, K., Wang, D., Mei, Z., 2023. Ecological impacts of unsustainable sand mining: urgent lessons learned from a critically endangered freshwater cetacean. Proc. R. Soc. B 290, 20221786.
Hu, J.Y., Xie, Y.H., Tang, Y., Li, F., Zou, Y.A., 2018. Changes of vegetation distribution in the east Dongting Lake after the operation of the three gorges dam. China. Front. Plant Sci. 9, 582. https://doi.org/10.3389/fpls.2018.00582.
Huang, S., Li, J., Xu, M., 2012. Water surface variations monitoring and flood hazard analysis in Dongting Lake area using long-term Terra/MODIS data time series. Nat. Hazards 62 (1), 93–100.
Huang, W., Liu, X., Tian, L., Cui, G., Liu, Y., 2024. Vegetation and carbon sink response to water level changes in a seasonal lake wetland. Front. Plant Sci. 15, 1445906. https://doi.org/10.3389/fpls.2024.1445906.
Intergovernmental Panel on Climate Change (IPCC), 2007. In: Solomon, S., et al. (Eds.), Climate Change 2007: The Physical Science Basis-Contribution of Working Group I to the Fourth Assessment Report of the Intergovernmental Panel on Climate Change. Cambridge Univ. Press, Cambridge, U. K, pp. 663–745.
Jiang, W., Hou, P., Zhu, X., Cao, G., Liu, X., Cao, R., 2011. Analysis of vegetation response to rainfall with satellite images in Dongting Lake. J. Geog. Sci. 21 (1), 135–149.
Jing, L., Zhou, Y., Zeng, Q., Liu, S., Lei, G., Lu, C., Wen, L., 2020. Exploring wetland dynamics in large river floodplain systems with unsupervised machine learning: a case study of the Dongting Lake. China. Remote. Sens. 12, 2995.
Kendall, M.G., 1970. Rank Correlation Methods. C. Griffin, London.
Kim, D.-K., Yang, C., Parsons, C.T., Bowman, J., T. Thëysmëyer, and G. B., Arhonditsis., 2021. Eutrophication management in a Great Lakes wetland: examination of the

existence of alternative ecological states. Ecosphere 12 (2), e03339. https://doi.org/10.1002/ecs2.3339.
Li, B., Wan, R., Yang, G., Yang, S., Dong, L., Cui, J., Zhang, T., 2024. Centennial loss of lake wetlands in the Yangtze plain, China: impacts of land use changes accompanied by hydrological connectivity loss. Water Res. 256, 121578.
Liu, Q., Liu, J., Liu, H., Liang, L., Cai, Y., Wang, X., Li, C., 2020. Vegetation dynamics under water-level fluctuations: implications for wetland restoration. J. Hydrol. 581, 124418. https://doi.org/10.1016/j.jhydr ol.2019.124418.
Liu, Y., Li, J., Yan, D., Chen, L., Li, M., Luan, Z., 2024. Typical vegetation dynamics and hydrological changes of Dongting Lake wetland from 1985 to 2020. Ecohydrology & Hydrobiology 24, 910–919.
Long, X., Li, X., Lin, H., Zhang, M., 2021. Mapping the vegetation distribution and dynamics of a wetland using adaptive-stacking and Google earth engine based on multi-source remote sensing data. Int. J. Appl. Earth Obs. Geoinformation 102, 102453.
Mann, H.B., 1945. Nonparametric tests against trend. Econometrica 13, 245–259.
Mei, X., Dai, Z., Fagherazzi, S., Chen, J., 2016. Dramatic variations in emergent wetland area in China's largest freshwater Lake, Poyang Lake. Adv. Water Resour. 96, 1–10.
Mu, S., Li, B., Yao, J., Yang, G., Wan, R., Xu, X., 2020. Monitoring the spatio-temporal dynamics of the wetland vegetation in Poyang Lake by Landsat and MODIS observations. Sci. Total Environ. 725, 138096.
Nyamweya, C., Lawrence, T.J., Ajode, M.Z., Smith, S., Achieng, A.O., Barasa, J.E., Masese, F.O., Taabu-Munyaho, A., Mahongo, S.B., Kayanda, R., Rukunya, E., Kisaka, L., Manyala, J.O., Medard, M., Otoung, S., Mrosso, H.D., Sekadende, B., Walakira, J., Mbabazi, S., Kishe, M.A., Shoko, A.P., Dadi, T., Gemmell, A., Nkalubo, W., 2023. Lake Victoria: overview of research needs and the way forward. J. Great Lakes Res 49, 102211.
Peng, D., Xiong, L., Guo, S., Shu, N., 2005. Study of Dongting Lake area variation and its influence on water level using MODIS data. Hydrol. Sci. J. 50 (1), 31–44.
Peng, H., Xia, H., Shi, Q., Chen, H., Chu, N., Liang, J., Gao, Z., 2022. Monitoring spatial and temporal dynamics of wetland vegetation and their response to hydrological conditions in a large seasonal lake with time series Landsat data. Ecol. Indic. 142, 109283.
People' s Government of Hunan Province, 2017. Sheng Shui Li Ting: Zi Ran Bao Hu Qu Nei Quan Mian Ji Zhi Cai Sha [Water Resources Department of Hunan Province: a total ban on sand mining in nature reserves].
Ramsar Convention on Wetlands, 2018. Global Wetland Outlook: State of the World's Wetlands and their Services to People. Ramsar Convention Secretariat, Gland, Switzerland.
Reynaud, A., Lanzanova, D., 2017. A global meta-analysis of the value of ecosystem services provided by lakes. Ecol. Econ. 137, 184–194.
Sterner, R.W., Keeler, B., Polasky, S., Poudel, R., Rhude, K., Rogers, M., 2020. Ecosystem services of earth's largest freshwater lakes. Ecosyst. Serv. 41, 101046.
Tan, Z., Li, Y., Zhang, Q., et al., 2022. Progress of hydrological Progress researches in Lake wetland: a review. Journal of Lake Sciences 34 (01), 18–37.
Wang, Y.M., Li, Z.W., Tang, Z.H., Zeng, G.M., 2011. A GIS-based spatial multi-criteria approach for flood risk assessment in Dongting Lake region, Hunan. Central China. Water Resour. Manag. 25, 3465–3484.
Wang, H., Bai, X., Huang, L., et al., 2024. The spatial variation of hydrological conditions and their impact on wetland vegetation in connected floodplain wetlands: Dongting Lake Basin. Environ. Sci. Pollut. Res. 31, 8483–8498. https://doi.org/10.1007/s11356-023-31673-4.
Xie, Y., Chen, X., 2008. Effects of three-gorge project on succession of wetland vegetation in dongting lake. Res. Agric. Modernization 29 (6), 684–687.
Xie, Y., Tang, Y., Chen, X., Li, F., Deng, Z., 2014. The impact of three gorges dam on the downstream eco-hydrological environment and vegetation distribution of east Dongting Lake. Ecohydrology 8 (4), 738–746.
Xing, L., Chi, L., Han, S., Wu, J., Zhang, J., Jiao, C., Zhou, X., 2022. Spatiotemporal dynamics of wetland in Dongting Lake based on multi-source satellite observation data during last two decades. Int. J. Environ. Res. Public Health 19 (21), 14180.
Xu, J., Wang, Y., Teng, M., Wang, P., Yan, Z., Wang, H., 2023. Ecosystem services of lake-wetlands exhibit significant spatiotemporal heterogeneity and scale effects in a multi-lake megacity. Ecol. Indic. 154.
Yang, L., Wang, L., Yu, D., Yao, R., Li, C., He, Q., Wang, S., Wang, L., 2020. Four decades of wetland changes in Dongting Lake using Landsat observations during 1978-2018. J. Hydrol. 587, 124954.
Yao, X., Zhu, J., Zeng, H., Yu, W., Zhang, H., 2022. Impact of accumulated temperature on wetland vegetation area in Poyang Lake. Computers, Materials & Continua 73 (1), 1915–1926. https://doi.org/10.32604/cmc.2022.026777.
Yao, F.F., et al., 2023. Satellites reveal widespread decline in global lake water storage. Science 380, 743–749. https://doi.org/10.1126/science.abo2812.
Yin, X., Yan, G., Wang, X., et al., 2022. Spatiotemporal distribution pattern of phytoplankton community and its Main driving factors in Dongting Lake, China-a seasonal study from 2017 to 2019. Water 14 (11), 1674.
Yin, P., Li, C., Wei, Y., Zhang, L., Liu, C., Chen, J., Liu, Y., Xiong, X., 2024. Impact of relative temperature changes on vegetation growth in China from 2001 to 2017. Journal of cleaner production 451, 142062. https://doi.org/10.1016/j.jclepro.2024.142062.
Yu, Y., Mei, X., Dai, Z., Gao, J., Li, J., Wang, J., Lou, Y., 2018. Hydromorphological processes of Dongting Lake in China between 1951 and 2014. J. Hydrol. 562, 254–266.
Yuan, Y., Zeng, G., Liang, J., Huang, L., Hua, S., Li, F., Zhu, Y., Wu, H., Liu, J., He, X., He, Y., 2015. Variation of water level in Dongting Lake over a 50-year period: implications for the impacts of anthropogenic and climatic factors. J. Hydrol. 525, 450–456.
Zhang, Y., Lai, X., Zhang, L., Song, K., Yao, X., Gu, L., Pang, C., 2020. The influence of aquatic vegetation on flow structure and sediment deposition: a field study in Dongting Lake. China. Journal of Hydrology 584, 124644.
Zhang, M., Lin, H., Long, X., Cai, Y., 2021. Analyzing the spatiotemporal pattern and driving factors of wetland vegetation changes using 2000-2019 time-series Landsat data. Sci. Total Environ. 780, 146615.
Zheng, S., Cheng, H., Tang, M., Xu, W., Liu, E., Gao, S., Best, J., Jiang, Y., Zhou, Q., 2022. Sand mining impact on Poyang Lake: a case study based on high-resolution bathymetry and sub-bottom data. J. Oceanol. Limnol. 40, 1404–1416.
Zhu, Y., Wang, H., Guo, W., 2021. The impacts of water level fluctuations of east Dongting Lake on habitat suitability of migratory birds. Ecol. Indic. 132, 108–277.